LANGMUIR

pubs.acs.org/Langmuir Article

Spontaneous and Ion-Specific Formation of Inverted Bilayers at Air/Aqueous Interface

Srikanth Nayak, Raju R. Kumal, and Ahmet Uysal*

Cite This: *Langmuir* 2022, 38, 5617−5625 Read Online

ACCESS | Metrics & More | Article Recommendations | Supporting Information

ABSTRACT: Developing better separation technologies for rare earth metals, an important aspect of a sustainable materials economy, is challenging due to their chemical similarities. Identifying molecular-scale interactions that amplify the subtle differences between the rare earths can be useful in developing new separation technologies. Here, we describe the ion-dependent monolayer to inverted bilayer transformation of extractant molecules at the air/aqueous interface. The inverted bilayers form with Lu^{3+} ions but not with Nd^{3+}. By introducing Lu^{3+} ions to preformed monolayers, we extract kinetic parameters corresponding to the monolayer to inverted bilayer conversion. Temperature-dependent studies show Arrhenius behavior with an energy barrier of 40 kcal/mol. The kinetics of monolayer to inverted bilayer conversion is also affected by the character of the background anion, although anions are expected to be repelled from the interface. Our results show the outsized importance of ion-specific effects on interfacial structure and kinetics, pointing to their role in chemical separation methods.

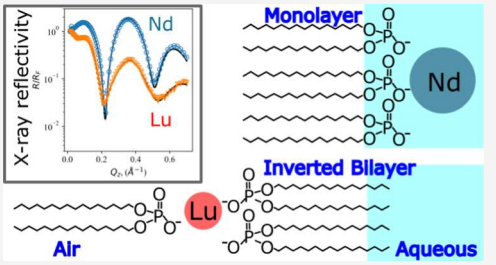

INTRODUCTION

Liquid−liquid extraction (LLE) is a chemical separation process widely used in hydrometallurgical processing of minerals, nuclear waste, and recycling.[1] Despite being used for decades, molecular-scale details of LLE are not well understood. A clear identification of free-energy drivers in LLE will lead to more efficient separation technologies, a crucial task due to the increasing demand for rare earths (REs), platinum group metals, and other critical materials.

LLE is a two-phase free-energy-driven process, involving complex ionic equilibria in both phases, interfacial effects, and solvent reorganization.[2,3] The selective interfacial transport of metallic ions is thought to be mainly driven by the amphiphilic extractant molecules used in LLE.[4] Dynamic structures forming at the liquid−liquid interface, such as water fingers, water ridges, and chemical "hinges" have been reported as some of the driving mechanisms for interfacial transport.[5−9] Self-assembly of extractant-ion aggregates at the interface can also play a dynamic role in the interfacial ion transport.[10] Thus, model systems focusing on the interfacial interactions of ions with amphiphilic molecules have been used to elucidate the processes in LLE.[11−20] In the context of LLE, ion−surfactant interactions at the air/aqueous interface can elucidate both the dynamic ion transport across the interface and the equilibrium structures formed by the ion−extractant complexes in the organic phase. Langmuir monolayers at the air−water interface are convenient model systems for LLE and have been well studied to probe intermolecular forces.[11,21] Influence of dissolved chemical species on monolayers has been studied to understand the intermolecular interactions in various biological and physicochemical systems.[22−25] Changes in the physical state of the interface are typically monitored by surface pressure isotherms, X-ray and neutron scattering techniques, vibrational spectroscopy, and light microscopy techniques.[21,25−28] However, a majority of these studies have been under static conditions, a drawback in understanding the kinetics of extractant−ion interactions in ion transport.

Dialkyl phosphoric acid extractants have been widely used in LLE of metals, particularly RE elements.[29] Bis(2-ethylhexyl) phosphoric acid (HDEHP) preferentially extracts the heavier lanthanides in a dimeric form such that there are six phosphate groups coordinating the extracted lanthanide in the organic phase.[30] Reverse micellar structures are formed in the organic phase after the extraction of metals with HDEHP.[31−34] Interfacial studies using vibrational sum frequency generation (VSFG) spectroscopy have shown the importance of hydrogen bonding interactions between the phosphate groups and water in stabilizing these micellar structures at the liquid−liquid interface.[10] Peak shifts in VSFG in the phosphate region induced by different lanthanides have been attributed to increasing interaction strength between HDEHP and the lanthanides with increasing atomic number.[35] Interestingly, interfacial X-ray scattering and fluorescence results suggest a preference for lighter lanthanides at the Gibbs monolayers of

Received: January 25, 2022
Revised: March 17, 2022
Published: April 28, 2022

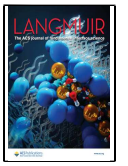

https://doi.org/10.1021/acs.langmuir.2c00208
Langmuir 2022, 38, 5617−5625

HDEHP at the air/aqueous interface, due to the higher solubility of HDEHP complexes of heavier lanthanides.[36]

Water-insoluble molecules, with longer alkyl tails, are limited to the interface and can plausibly provide more information on the ion−extractant interactions. Dihexadecylphosphate (DHDP) forms an insoluble monolayer on water, and it has been used as an analogue of HDEHP for this purpose.[12,20,37] At the dodecane−water interface, "kinetically arrested" inverted bilayer of DHDP-Er(III) complexes has been observed.[13,37] This phenomenon was proposed to underlie the micellization in the organic phases after LLE.[13]

Here, we show that the inverted bilayers of DHDP can be created at air/aqueous interface, allowing kinetic and temperature-dependent studies. Using synchrotron X-ray scattering techniques and VSFG, we first show that the inverted bilayers form with Lu^{3+}, but not with Nd^{3+}, chemically very similar lanthanides, which shows that the charge density of the metal ion is the main driver behind the inverted bilayer formation (Figure 1). Bilayers can form regardless of the monolayer

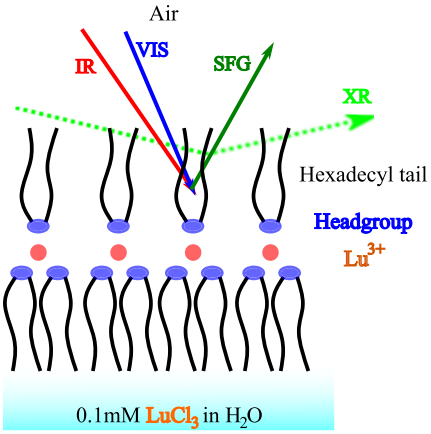

Figure 1. Schematic depiction of the experiments to probe the interaction of DHDP molecules with Lu^{3+} ions at the air/aqueous interface. Samples are prepared by spreading DHDP on aqueous solutions of trivalent ions (See SI Methods). Specular XR and VSFG are complementary techniques that provide surface-specific structural information.

spreading procedure: (a) when DHDP is spread on Lu^{3+}-containing solutions, inverted bilayers form immediately, (b) when DHDP monolayer is spread on pure water and Lu^{3+} ions are introduced later, the monolayer transforms into an inverted bilayer spontaneously. Temperature-dependent studies determined that the monolayer to inverted bilayer transition follows first-order kinetics with an Arrhenius behavior. Very interestingly, background anions, such as nitrate and thiocyanate, significantly affect the bilayer formation kinetics, although they are expected to be repelled from the interface due to electrostatic interactions. We discuss the static monolayer and bilayer structures in detail and investigate the kinetics of bilayer formation with multiple probes.

RESULTS AND DISCUSSION

Figure 2a shows the isotherms obtained by the compression of DHDP-covered surfaces, a common method to study Langmuir monolayers,[21] in the presence of either of the lanthanide ions. In the presence of Nd^{3+}, the surface pressure increases rapidly as the surface area is compressed to ∼41 Å^2 per DHDP. This is typical for a monolayer of double-chain molecule, considering that the molecular area for a single hydrocarbon tail is ∼20 Å^2. In contrast, in the presence of Lu^{3+} in the subphase, the surface pressure begins to rise at much lower values of surface area per DHDP. The lower area per DHDP (∼25 Å^2) in the presence of Lu^{3+} suggests the formation of a bilayer or multilayer at the surface.

The interfacial structure can be resolved by specular X-ray reflectivity (XR) as it provides information on the electron density profile (EDP) normal to the surface.[38,39] Figure 2b shows the Fresnel-normalized XR obtained for DHDP-covered surfaces in the presence of Nd^{3+} and Lu^{3+}. There are major qualitative differences in the reflectivity curves—with Nd^{3+}, the normalized reflectivity increases at low Q_z, whereas it decreases in the presence of Lu^{3+}. Further, the first extremum occurs at a smaller Q_z for Lu^{3+} surfaces. EDPs obtained from the box-model fits to the reflectivity curves are shown in Figure 2c,d. The fit parameters are given in Table S2 that provide information on the thickness of the layer (d), electron density (ρ), and roughness (σ). The interfacial region is wider in the case of Lu^{3+} compared to that of Nd^{3+}, which matches with the corresponding lower period of oscillations in the reflectivity curve. The EDP for the Nd^{3+} sample precisely follows the expected profile for a monolayer, similar to those obtained with La^{3+}.[40] The boxes used in the fit correspond to the expected physical properties of the system—tail group region with a thickness of ∼20 Å and electron density ∼0.29 e/Å^3 corresponding to a closely packed alkyl chain region. The integrated electron density of the headgroup region is ∼2.5 e/Å^2 which includes contributions from the phosphate groups, adsorbed Nd^{3+}, and water molecules. In the case of Lu^{3+}, the EDP suggests an inverted bilayer structure. However, the boxes do not appear to have one-to-one correspondence with the ideal molecular structure, which is expected due to possible interdigitation in the bilayer structure and the roughness of the interface. So, we perform an empirical analysis of the EDP as below.

We ascribe the peak in EDP (at $z \sim -30$ Å) to a layer of Lu^{3+} ions (Figure 2d, orange). For a regular bilayer, the electron density should uniformly decrease from this Lu^{3+} layer to the bulk aqueous region. The presence of a lower density region in the EDP between this Lu^{3+} layer and the aqueous bulk region ($\rho \sim 0.33$) suggests the presence of alkane chains, which in turn indicates that the surface is covered with an inverted bilayer. There can be two canonical conformations for the inverted bilayer − two DHDP molecules exposed to the air side and one toward the aqueous side, or vice versa. We can decompose the EDP shown in Figure 2d into three regions—top, middle, and bottom layers (Figure 2d, blue, orange, and green). We assume that the DHDP tail groups are fully extended in both top and bottom layers. This assumption is supported by the absence of any gauche defects (2850 cm^{-1} band) in the alkyl chains as shown by the VSFG spectra (Figure 3). Thus, we make the top and bottom layers to have approximately 20 Å thickness, which corresponds to the full length of all-trans hexadecyl chains. This gives us an integrated electron density of ∼3.1, 6.9, and 6.7 e/Å^2 for top, middle, and bottom layers, respectively. The higher electron density of the bottom layer than the top layer suggests that there are more DHDP molecules adjacent to the aqueous side. This conformation is favored possibly due to the higher shielding of water from the chains with a tightly packed alkyl chain layer compared to a loosely packed alkyl chain region.

https://doi.org/10.1021/acs.langmuir.2c00208
Langmuir 2022, 38, 5617−5625

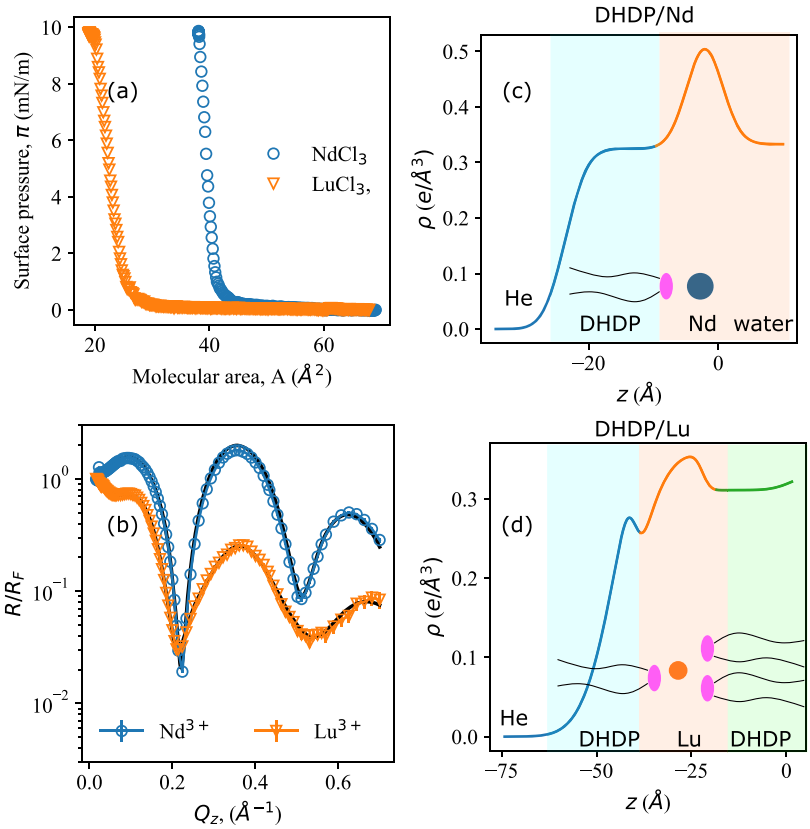

Figure 2. (a) Langmuir isotherms showing the formation of a monolayer of DHDP on the surface of 0.1 mM $NdCl_3$ solution (blue circles), and an inverted bilayer on the surface of 0.1 mM $LuCl_3$ solution (orange triangles). (b) X-ray reflectivity results for 0.1 mM $NdCl_3$ (blue circles) and 0.1 mM $LuCl_3$ in water (orange triangles) and the corresponding EDPs in (c) and (d). The fits for $NdCl_3$ were obtained using a two-box model corresponding to the monolayer tail region and the headgroup region. The fits for $LuCl_3$ were obtained with a three-box model, and it shows the formation of an inverted bilayer at the air/aqueous interface. Schematics of the interfacial structure with Nd^{3+} and Lu^{3+} are also shown in (c) and (d).

VSFG experiments provide further confirmation for the suggested bilayer structure. VSFG spectrum of the DHDP-Lu^{3+} system shows a decrease in CH_3 stretch peak intensity compared to DHDP-water case, indicating lower asymmetry relative to a monolayer (Figure 3a). Since VSFG is a dipole-forbidden process, molecules orienting opposite to each other either cancel or reduce the net dipole and lower the intensity. If the bilayer is symmetrical, having equal number of the DHDP molecules on top and bottom, the overall peak intensity would reduce to zero. Thus, our VSFG results support the XR results showing unequal distribution of DHDP between the top and bottom layers. In the presence of Nd^{3+} ions, there is no decrease in intensity confirming the monolayer structure. In fact, the signal slightly increases due to the better packing of the molecules as the headgroup charge is shielded by the adsorbed ions, reducing the repulsion. The corresponding spectra in the OH region provide information on the interfacial water structure (Figure 3b). On pure water, the electric field of the headgroups orients the water molecules, inducing a strong VSFG signal. In the case of Nd^{3+}, ions shield the charge of the headgroup diminishing the VSFG signal.[14,41] In the case of Lu^{3+}, inverted bilayer forms and the tails touching the surface do not create any significant orientational ordering of water molecules.

We can directly detect the metal ions in monolayer and inverted bilayer structures by X-ray fluorescence near total reflection (XFNTR).[15,38] Figure S3 shows the variation of integrated fluorescence signal in the L_α region of Nd and Lu as a function of the vertical momentum transfer (Q_z). The fits to the data provide an estimate of the interfacial number density of the elements (Table S1). For Nd^{3+}, we obtain an area of ~110 ± 5 Å^2 per Nd. At ~41 Å^2 per DHDP molecule, there is ~0.36 ± 0.02 Nd^{3+} per DHDP, which is close to the Nd^{3+} number density required for balancing the charge of the monolayer. With Lu^{3+}, however, we obtain 37 ± 4 Å^2 per Lu, or approximately 0.68 Lu per DHDP molecule at 25 Å^2 per DHDP. Assuming that the charge balance is satisfied only by DHDP and Lu^{3+} ions, the minimum surface area per Lu^{3+} when both the top and bottom DHDP layers are fully packed should be 120 Å^2/2 = 60 Å^2. As the obtained surface area is significantly less than this minimum, the speciation of Lu is probably different from the trivalent species found in bulk solution, i.e., counterions may be present in the bilayer to compensate the charge. The presence of divalent hydroxyl-lanthanide species next to an anionic monolayer has been recently reported.[42]

In the absence of any Lu^{3+} ions, DHDP forms a monolayer on water, and this provides an opportunity to study the kinetics of the bilayer formation. XR of the interface after compressing DHDP on water to a surface pressure of 10 mN/m shows the formation of a monolayer (Figure 4, blue). Upon introduction of Lu^{3+} ions in the subphase, behind the trough barrier, the X-ray reflectivity shows a gradual change along with decrease in surface area for maintaining constant surface pressure. About

https://doi.org/10.1021/acs.langmuir.2c00208
Langmuir 2022, 38, 5617−5625

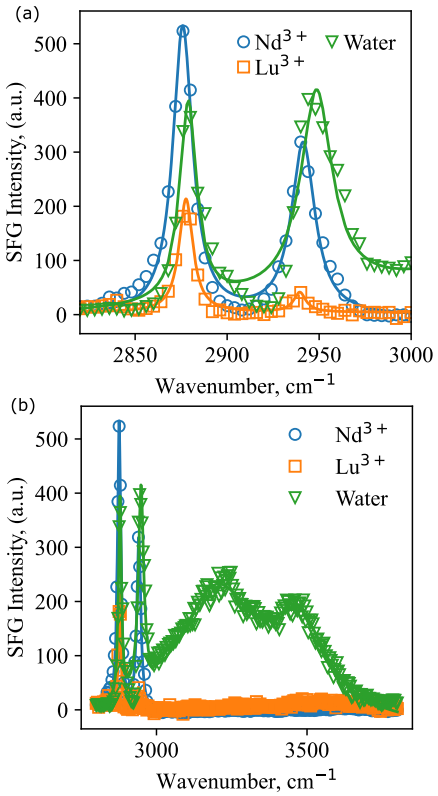

Figure 3. SFG spectra of DHDP/aqueous interface in the presence and absence of lanthanide ions showing (a) CH_2 and CH_3 stretch regions, and (b) CH_2, CH_3 and OH stretch region. The concentration of lanthanide ions in all of the systems is 0.1 mM.

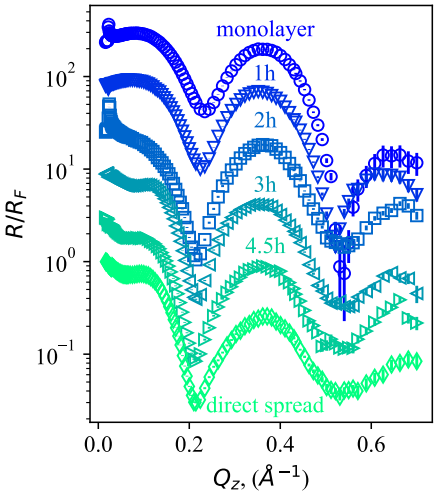

Figure 4. Time-dependent variation of the Fresnel-normalized XR profile of the DHDP-covered surface upon introduction of Lu^{3+} to the subphase. DHDP is spread on water and is compressed to form a monolayer at a surface pressure of 10 mN/m. At $t = 0$, a small volume of $LuCl_3$ solution is injected into the subphase, behind the trough barrier. The monolayer begins to shrink in area while maintaining a constant surface pressure (see Figure 5a for the surface pressure isotherm). After ~4.5 h, the XR profile of the surface resembles that of DHDP spread directly on the $LuCl_3$ solution (Figure 2b). The XR curves at different time stamps have been shifted vertically for clarity.

4.5 h after the introduction of Lu^{3+}, the XR curve becomes very similar to the one shown in Figure 2b, indicating that the interface has an inverted bilayer structure similar to the one obtained by the direct spreading of DHDP on Lu^{3+}-containing subphase (Figure 4, green).

The effect of monovalent anions on the interfacial adsorption and transport of lanthanides has been reported earlier.[14,15,43] We found no effect of background ions on the final static structure or XFNTR results when spreading DHDP on the subphase containing lanthanides and background salts (Figures S3 and S4). However, there is an anion dependence in the kinetics of monolayer to the inverted bilayer transition (Figure 5) upon addition of Lu^{3+}. We spread DHDP

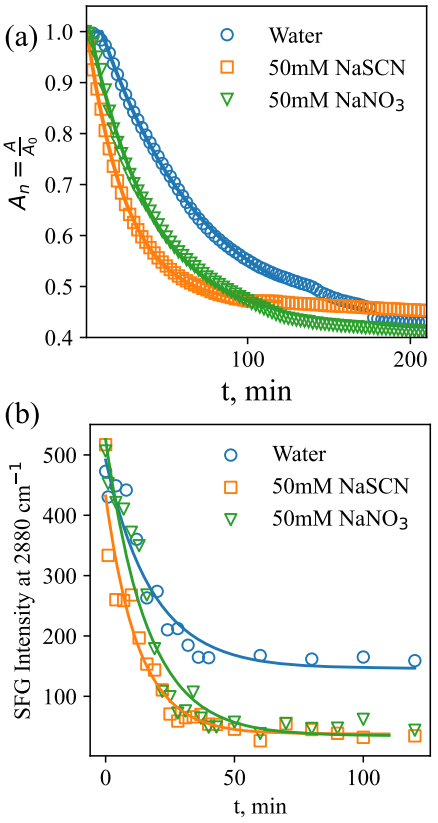

Figure 5. (a) Kinetics of the formation of inverted bilayer are dependent on the background anion present in the aqueous subphase. Thiocyanate (orange squares) leads to a faster formation of the bilayer compared to nitrate (green triangles), both faster than having no background salt (blue circles). The solid lines are fits to an empirical model based on nucleation growth theory shown in eq 1. (b) Decay rates of the amplitude of the CH_3 symmetric stretch peak from VSFG experiments also indicate that the monolayer to inverted bilayer transition is faster in the presence of NaSCN.

monolayer on salt solutions (0.1 M of $NaNO_3$ or NaSCN) and introduced either Nd^{3+} or Lu^{3+} solution behind the barrier (Figure S2). The barrier position was allowed to move to maintain a constant surface pressure of 10 mN/m, the same as the one used above. With the introduction of Nd^{3+}, the surface area remains constant with time (Figure S5). Figure 5a shows the decay of trough area required to maintain the surface pressure constant upon injecting Lu^{3+} solution. We have modeled the decay as an exponential function of time according to eq 1. This model has three parameters: t_0 (time offset after which the decay is exponential), k (rate constant for exponential decay), and a_∞ (the ratio of final to initial trough area). The fit parameters are listed in Table S3. The rate of decay roughly corresponds to the monolayer to inverted

https://doi.org/10.1021/acs.langmuir.2c00208
Langmuir 2022, 38, 5617−5625

bilayer transition. Thus, there is an effect of background anion on the monolayer to inverted bilayer transition. Both nitrate and thiocyanate increase the rate of transition with thiocyanate having a stronger effect.

The intensity of CH_3 symmetric stretch peak in VSFG spectra, at 2875 cm^{-1}, provides a molecular-scale description of monolayer to bilayer transition (Figures 3 and S6). Figure 5b shows the decay of this peak upon the introduction of Lu^{3+} to the subphases below DHDP monolayers. An exponential decay model was used to fit the data (solid lines in Figure 5b), and the parameters are listed in Table S4. The rate of monolayer to inverted bilayer conversion is increased by background ions, and thiocyanate has a stronger effect than nitrate. The rate of conversion obtained from VSFG appears to be faster than the corresponding rates obtained by surface pressure isotherms. There may be a few reasons for the difference. First, VSFG probes the molecular-scale structure directly, as opposed to the macroscopic surface area measurement. Also, a constant area setup used in VSFG versus the constant pressure setup in the isotherms can contribute to the differences (Figure S2). We note that the intensity of CH_3 symmetric stretch peak does not significantly change upon introducing Nd^{3+} ions to the subphase (Figure S7).

We investigated the temperature dependence of monolayer to bilayer transition to understand the energetics of the process (Figure 6a). The rate constant is derived from the fits to an empirical model based on the classical nucleation growth theory (eq S1). Its variation as a function of the inverse temperature is shown in Figure 6b. The fit parameters are tabulated in Table S3. The linear relationship shows that the monolayer to inverted bilayer transition follows the Arrhenius equation. We obtain an activation energy of ~40 kcal/mol for the transition. The induction time for monolayer to inverted bilayer transition (t_0) decreases with increasing temperature.

Anion- and temperature-dependent studies are briefly described here, as a proof of concept, to demonstrate that we can elucidate the kinetics of amphiphile−ion interactions and obtain information that is not available in static measurements. More detailed studies utilizing these approaches will follow.

We have studied the differences in Lu^{3+} and Nd^{3+} adsorption onto DHDP-laden aqueous surfaces using X-ray scattering, VSFG, and surface pressure isotherms. Regardless of the surface preparation method, DHDP forms an inverted bilayer structure in the presence of Lu^{3+} ions and a monolayer in the presence of Nd^{3+} ions (Figure 7). The qualitative difference between the nanoscale structures induced by different charge densities of Nd^{3+} and Lu^{3+} directly affects the macroscopic system, a desirable feature in chemical separations. The ion-specific formation of inverted bilayer with Lu^{3+} indicates a difference in kinetics of ion transfer with lighter and heavier lanthanides even at longer time scales than that were investigated by simulations.

All of the RE ions are predominantly +3 charged, and the main difference between them is in their ionic sizes, which decreases with atomic number for a given coordination number.[44,45] The chemistry of REs is dominated by electrostatic interactions in the solid state.[46,47] In solutions, the mean-field theories developed for monovalent ions at dilute concentrations[48−50] usually fail to describe experimental observations with RE ions which are multivalent. At surfaces, multivalent ions can induce "charge-reversal" or spontaneous collapse of monolayers, phenomena that are not observed with monovalent ions.[51,52] In this context, effects of ion−ion and ion−surfactant correlations and specific interactions between ions and surfactants, such as hydrogen bonds and coordination bonds, have been described.[11,40,53,54] Our results add a new

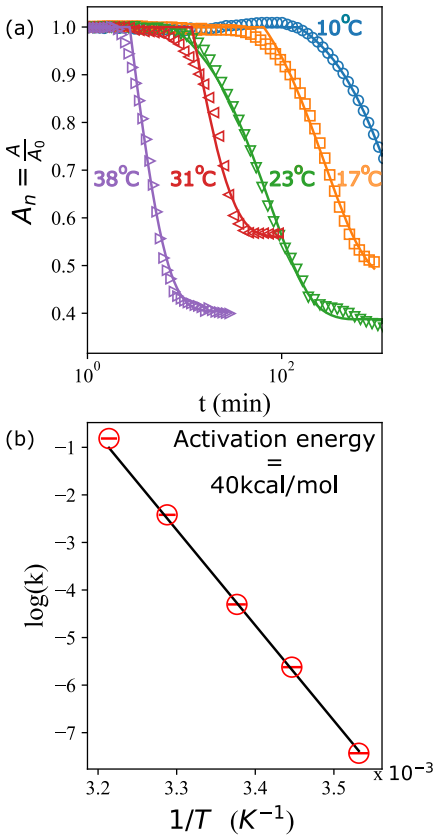

Figure 6. (a) Temperature dependence of the normalized area that is required to maintain a constant surface pressure of 10 mN/m as a function of time with injection of $LuCl_3$ to the subphase (final concentration of 0.1 mM). While at a low temperature of 10 °C, the compression of the surface due to the formation of the bilayer occurs in the scale of hours, at 38 °C, the transition occurs within minutes. Black solid lines show the fits obtained using an exponential decay, corresponding to the first-order kinetics of the transition (eq S1). (b) Variation of the first-order rate constant (k) of monolayer−bilayer transition shows a classical Arrhenius type of behavior.

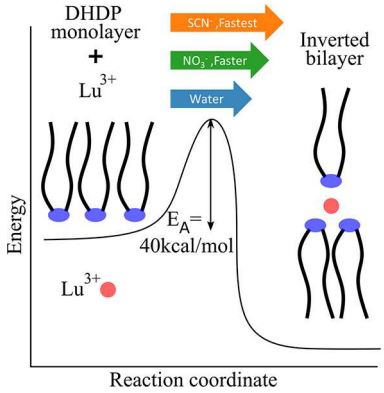

Figure 7. Schematic description of the monolayer to inverted bilayer transition of DHDP in the presence of Lu^{3+} ions based on Figures 5 and 6. The reaction follows first-order kinetics with an energy barrier of 40 kcal/mol and is catalyzed by background anions—SCN^- and NO_3^-.

https://doi.org/10.1021/acs.langmuir.2c00208
Langmuir 2022, 38, 5617−5625

dimension to these observations and show that the complex interactions of the trivalent ions can be fine-tuned to create qualitative differences in their interactions with amphiphiles, which directly affects the macroscopic behavior of the system.

Our results with DHDP at air−water interface and the prior results obtained with DHDP at water−dodecane interface show that an inverted bilayer of DHDP is formed with heavy, charge-dense trivalent ions.[13,37] The dodecane−water interface experiments required lower temperatures to kinetically arrest the interfacial species formed during ion transfer. At the dodecane−water interface, Sr^{2+} adsorbs to a monolayer of DHDP.[12] This difference between trivalent and divalent ions was interpreted as different extraction mechanisms for them with dialkyl phosphoric acid extractants.[13] Our results suggest that it is not necessarily a difference between divalent and trivalent ions, but possibly a difference in charge densities as DHDP forms a monolayer under both Nd^{3+} and Sr^{2+}.

We note that DHDP is used as an interfacial analogue to HDEHP in our study. It is important to consider the effects of tail structure. In LLE, the tail group plays a major role in extraction, organic phase structure, and phase behavior.[55−58] Similarly, the tail structure plays a major role in the formation and structure of the Langmuir monolayers due to the van der Waals interactions between the tails.[21,59,60] In contrast to the results obtained with DHDP, VSFG studies with HDEHP at the air−water interface suggest that HDEHP interacts with all of the lanthanides in a monolayer-like structure.[35,61] Similarly, XR of the HDEHP at the air−water interface is not qualitatively different for light and heavy lanthanides.[36] With a shorter chain analogue of HDEHP, namely, dibutyl phosphate, a structure similar to inverted bilayer is observed.[61] Organic phase speciation of Er is also different when extracted with HDEHP (hexamer) or DHDP (trimer).[37] Regardless of these differences, it is evident that the small changes in ionic size of the lanthanides can have major implications to the organic phase structure and thereby the extraction energetics.

Although there are several studies on the collapse of Langmuir monolayers due to compression,[62−65] there are fewer on the spontaneous collapse of monolayers induced by solutes. Recently, a spontaneous monolayer to inverted bilayer transformation of palmitic acid in the presence of calcium ions has been reported.[52] Divalent cations have also been shown to reduce the surface pressure at which stearic acid films collapse.[66] Such interplay of ion−lipid interactions is especially important in the biophysics of cellular membranes where lipids affect selective ion transport and ions affect transbilayer lipid motions.[67−72] In this context, a coordination-driven, ion-specific monolayer to inverted bilayer transition has been reported with calix[4]arene films on Cu(II) or Ni(II) solutions.[73] Unlike the lanthanide ions where ligands interact electrostatically, transition metals can show significant selectivities due to ligand−metal coordination bonds that are directional. Finally, a paper published while our manuscript was under review confirms the static inverted bilayer structure we propose for the lutetium system.[74]

The kinetics of monolayer to inverted bilayer transition with Lu^{3+} in the subphase is strongly temperature-dependent with an activation barrier of ∼40 kcal/mol. This relatively large energy barrier is in correspondence with the low temperature required to arrest the heavy lanthanide species at the dodecane−water interface.[37] The onset of transition is also temperature-dependent, indicating a temperature-dependent nucleation of inverted bilayer structure. The transformation of monolayer to inverted bilayer probably involves multiple steps with a first-order rate-limiting step that is captured in our kinetic studies. DHDP forms stable monolayers with Nd^{3+} in the subphase at temperatures up to 37 °C. Whether inverted bilayers can form with lighter lanthanides at higher temperatures is an open question. It is not clear whether inverted bilayer formation with Nd^{3+} is kinetically limited or is thermodynamically unstable.

We have previously reported the anion dependence in lanthanide adsorption at DHDP monolayers.[15] These experiments were conducted with preformed monolayers and lanthanide injection behind the barrier. Under the impression that the surfaces were under equilibrium, we attributed the differences in fluorescence signals to the effect of anion on the number density of lanthanides adsorbing to the surface. We obtained an interfacial area per Lu that is lower than that for 1:3 Lu:DHDP complexes and interpreted that to be a result of excess background anions. This present report shows that the lower interfacial area per Lu is obtained even in the absence of background salts. Further, the reported difference in Lu adsorption with different background salts is due to the differences in kinetics of inverted bilayer formation in the presence of NO_3^- and SCN^-.

CONCLUSIONS

We have demonstrated how monolayer to bilayer conversion can be used to identify important ion-specific effects in RE separations. Phosphoric acid-based extractants are often used in the LLE of RE elements, but there are outstanding questions on the mechanisms that determine ion transport and selectivity. Here, we have shown that there is an ion-specific effect in the adsorption of trivalent ions to DHDP, an analogue of phosphoric acid-based extractants: larger trivalent ion Nd^{3+} maintains the monolayer structure of DHDP, while smaller Lu^{3+} ion induces the formation of an inverted bilayer. This shows that the air/aqueous interface models can be used to reproduce important aspects of oil/water interfaces. Further, the monolayer of DHDP collapses to an inverted bilayer upon the introduction of Lu^{3+} ions where the rate of collapse is temperature-dependent. These results show that the minor differences in ionic sizes of the RE elements have major impacts on the interfacial structure. Elucidating these effects at the air−water interface can show the drivers of ion transport and selectivity in LLE. The kinetics of ion-dependent monolayer to inverted bilayer transition provide a route to investigate ion transport and lipid structure in various physicochemical processes.

EXPERIMENTAL METHODS

Materials. Dihexadecylphosphate (DHDP) was purchased from Avanti Polar Lipids, Inc. Neodymium (III) chloride hexahydrate, lutetium (III) chloride hexahydrate, sodium chloride, sodium nitrate, and sodium thiocyanate were purchased from Sigma-Aldrich, Inc., and used as received without any further purification. Aqueous solutions of lanthanides and sodium salts were prepared in volumetric flasks. DHDP was dissolved in chloroform to prepare a 0.25 mM solution. The pH of the solutions was 5.8 ± 0.1.

Sample Preparation for Static Studies. X-ray scattering studies were conducted at sector 15-ID-C of Advanced Photon Source, Argonne National Laboratory. In a typical experiment, the aqueous subphase containing lanthanides was poured into the Langmuir trough placed in a sealable chamber. The liquid surface was compressed and aspirated as a surface preparation step. With the barrier in the "open" position, a measured volume of DHDP solution

https://doi.org/10.1021/acs.langmuir.2c00208
Langmuir 2022, 38, 5617−5625

was spread on the surface, dropwise, with a 100 μL glass Hamilton syringe. The surface was then compressed by moving the motorized barrier at 8 cm^2/min to reach a surface pressure of 10 mN/m. The surface is kept under this constant pressure by barrier motion controlled with a NIMA IU4 controller. The chamber was then sealed and purged with water-saturated He gas.

The VSFG studies were conducted in a fixed area mode. Approximately 40 mL of the aqueous subphase is poured into a shallow PTFE dish with a circular cross-section (diameter = 10 cm). Droplets of DHDP solution were spread on the surface of the liquid slowly using a 10 μL Hamilton syringe while monitoring the surface pressure. Enough droplets were added to achieve a surface pressure of 10 mN/m.

Sample Preparation for Kinetic Studies. For X-ray scattering experiments, 198 mL of lanthanide-free aqueous subphase (water or a salt solution) was poured into the trough and DHDP was spread on the liquid surface. The monolayer was compressed to a surface pressure of 10 mN/m. After the formation of a stable monolayer, 2 mL of the lanthanide solution at an appropriate concentration was added to the subphase by injecting the solution behind the trough barrier using a plastic syringe. The subphase was then mixed by pumping the solution in and out of the syringe for 10 min at a rate of ~45 mL/min

For temperature-dependent kinetic studies, the trough temperature was controlled by pumping an ethylene glycol solution (~5 wt %) that was cooled or heated with a NESLAB RTE 111 chiller. The temperature of the subphase was measured using a thermocouple.

We used the following empirical model based on the classical nucleation growth theory[75] to fit the decay of the trough area required to hold a constant surface pressure in the presence of Lu^{3+} ions as follows

$$\frac{a(t) - a_\infty}{1 - a_\infty} = u(t - t_0)(e^{-k(t-t_0)}) + u(t_0 - t) \quad (1)$$

where $a(t)$ is the ratio of the area at a given time to the initial monolayer area, k is the exponential decay rate constant, t_0 is the time delay between the introduction of Lu^{3+} and the onset of exponential decay, a_∞ is the area ratio at steady state, and $u(x)$ is the Heaviside function.

Synchrotron X-ray Studies. XR and XFNTR studies were conducted at sector 15-ID-C of Advanced Photon Source, Argonne National Laboratory as described in our previous papers.[14,41] X-ray energy was set to 18.3 keV above the L3 absorption edges of Lu and Nd. A Dectris PILATUS 100 detector was used for obtaining reflected X-ray intensity. At each incident angle, a background signal was subtracted from the reflection. The XR data were fit using Stochfit.[76] XFNTR data were collected using an energy-dispersive Vortex detector setup normal to the surface with a collection snout placed ~10.6 mm from the surface. At each incidence angle, Gaussian curves were fit to the fluorescence spectra corresponding to the element of interest. Integrals of the peaks are used in the XFNTR figures.

VSFG Experiments. The VSFG measurements are acquired using an EKSPLA system, which has been described previously.[14,16,17,41] Briefly, an amplified Nd:YAG laser system produces 29 ps pulses having 28 mJ energy centered at 1064 nm with a repetition rate of 50 Hz. The harmonic unit splits the 1064 nm laser and generates two beams of 532 nm. A fundamental laser beam 1064 nm and a second harmonic beam 532 nm are used to generate a narrowband IR pulse tunable from 1000 to 4000 cm^{-1} via an optical parametric generator and difference frequency generation. The other 532 nm laser beam is used as a visible source to generate VSFG signal. The SFG signal is passed through a monochromator and collected using a photomultiplier tube.

The VSFG measurement is carried out using a reflection geometry where the incident angles of the visible and IR beams are 60 and 55°, respectively, to the surface normal. The visible light is attenuated to an average energy of 600 μJ, and the IR energy is maintained at 100 μJ for all measurements. A motorized piezoelectric rotation stage is used to rotate the sample to avoid beam damage. Each spectrum is collected with a 4 cm^{-1} increment over the range of 2800−3800 cm^{-1} and averaged over 300 laser shots per point. The spectra are collected under various polarization combinations and are normalized against the SFG spectrum of a z-cut quartz.

■ ASSOCIATED CONTENT

Supporting Information

The Supporting Information is available free of charge at https://pubs.acs.org/doi/10.1021/acs.langmuir.2c00208.

VSFG spectra showing the OH region, results from X-ray fluorescence near total reflection, X-ray reflectivity curves in the presence of salts, surface pressure isotherm of DHDP on Nd^{3+} solution showing its stability, and fit parameters for the empirical model describing the kinetics of monolayer to inverted bilayer transition (PDF)

■ AUTHOR INFORMATION

Corresponding Author

Ahmet Uysal − *Chemical Sciences and Engineering Division, Argonne National Laboratory, Lemont, Illinois 60439, United States;* orcid.org/0000-0003-3278-5570; Email: ahmet@anl.gov

Authors

Srikanth Nayak − *Chemical Sciences and Engineering Division, Argonne National Laboratory, Lemont, Illinois 60439, United States;* orcid.org/0000-0003-0213-5796

Raju R. Kumal − *Chemical Sciences and Engineering Division, Argonne National Laboratory, Lemont, Illinois 60439, United States;* orcid.org/0000-0002-6077-8741

Complete contact information is available at: https://pubs.acs.org/10.1021/acs.langmuir.2c00208

Author Contributions

The manuscript was written through contributions of all authors. All authors have given approval to the final version of the manuscript.

Notes

The authors declare no competing financial interest.

■ ACKNOWLEDGMENTS

The authors thank Wei Bu for his help with the liquid surface synchrotron experiments. This work was supported by the U.S. Department of Energy, Office of Basic Energy Science, Division of Chemical Sciences, Geosciences, and Biosciences, Separation Science program under contract DE-AC02-06CH11357. Use of the Advanced Photon Source, an Office of Science User Facility operated for the U.S. Department of Energy (DOE) Office of Science by Argonne National Laboratory, was supported by the U.S. DOE under Contract No. DE-AC02-06CH11357. NSF's ChemMatCARS Sector 15 is principally supported by the Divisions of Chemistry (CHE) and Materials Research (DMR), National Science Foundation, under Grant NSF/CHE-1834750.

■ ABBREVIATIONS USED

XFNTR, X-ray fluorescence near total reflection; VSFG, vibrational sum frequency generation; LLE, liquid−liquid extraction; XR, X-ray reflectivity; DHDP, dihexadecylphosphate

REFERENCES

(1) Moyer, B. *Changing the Landscape in Solvent Extraction*, 1st ed.; CRC Press: Boca Raton, 2020; Vol. *23*, p. 310.
(2) Wilson, A. M.; Bailey, P. J.; Tasker, P. A.; Turkington, J. R.; Grant, R. A.; Love, J. B. Solvent extraction: the coordination chemistry behind extractive metallurgy. *Chem. Soc. Rev.* **2014**, *43*, 123−134.
(3) Nelson, J. J. M.; Schelter, E. J. Sustainable Inorganic Chemistry: Metal Separations for Recycling. *Inorg. Chem.* **2019**, *58*, 979−990.
(4) Clark, A. E. Amphiphile-Based Complex Fluids: The Self-Assembly Ensemble as Protagonist. *ACS Cent. Sci.* **2019**, *5*, 10−12.
(5) Kikkawa, N.; Wang, L.; Morita, A. Microscopic Barrier Mechanism of Ion Transport through Liquid-Liquid Interface. *J. Am. Chem. Soc.* **2015**, *137*, 8022−8025.
(6) Wen, B.; Sun, C.; Zheng, W.; Bai, B.; Lichtfouse, E. Evidence for water ridges at oil-water interfaces: implications for ion transport. *Soft Matter* **2020**, *16*, 826−832.
(7) Qiao, B.; Muntean, J. V.; Olvera de la Cruz, M.; Ellis, R. J. Ion Transport Mechanisms in Liquid-Liquid Interface. *Langmuir* **2017**, *33*, 6135−6142.
(8) Benjamin, L. Mechanism and dynamics of ion transfer across a liquid-liquid interface. *Science* **1993**, *261*, 1558−1560.
(9) Liu, Z.; Clark, A. E. An octanol hinge opens the door to water transport. *Chem. Sci.* **2021**, *12*, 2294−2303.
(10) Chowdhury, A. U.; Lin, L.; Doughty, B. Hydrogen-Bond-Driven Chemical Separations: Elucidating the Interfacial Steps of Self-Assembly in Solvent Extraction. *ACS Appl. Mater. Interfaces* **2020**, *12*, 32119−32130.
(11) Miller, M.; Liang, Y.; Li, H.; Chu, M.; Yoo, S.; Bu, W.; Olvera de la Cruz, M.; Dutta, P. Electrostatic Origin of Element Selectivity during Rare Earth Adsorption. *Phys. Rev. Lett.* **2019**, *122*, No. 058001.
(12) Bu, W.; Mihaylov, M.; Amoanu, D.; Lin, B. H.; Meron, M.; Kuzmenko, I.; Soderholm, L.; Schlossman, M. L. X-ray Studies of Interfacial Strontium-Extractant Complexes in a Model Solvent Extraction System. *J. Phys. Chem. B* **2014**, *118*, 12486−12500.
(13) Liang, Z.; Bu, W.; Schweighofer, K. J.; Walwark, D. J.; Harvey, J. S.; Hanlon, G. R.; Amoanu, D.; Erol, C.; Benjamin, I.; Schlossman, M. L. Nanoscale view of assisted ion transport across the liquid−liquid interface. *Proc. Natl. Acad. Sci. U.S.A.* **2019**, *116*, 18227−18232.
(14) Lovering, K.; Nayak, S.; Bu, W.; Uysal, A. The Role of Specific Ion Effects in Ion Transport: The Case of Nitrate and Thiocyanate. *J. Phys. Chem. C* **2020**, *124*, 573−581.
(15) Nayak, S.; Lovering, K.; Bu, W.; Uysal, A. Anions Enhance Rare Earth Adsorption at Negatively Charged Surfaces. *J. Phys. Chem. Lett.* **2020**, *11*, 4436−4442.
(16) Nayak, S.; Kumal, R. R.; Liu, Z.; Qiao, B.; Clark, A. E.; Uysal, A. Origins of Clustering of Metalate-Extractant Complexes in Liquid-Liquid Extraction. *ACS Appl. Mater. Interfaces* **2021**, *13*, 24194−24206.
(17) Rock, W.; Qiao, B. F.; Zhou, T. C.; Clark, A. E.; Uysal, A. Heavy Anionic Complex Creates a Unique Water Structure at a Soft Charged Interface. *J. Phys. Chem. C* **2018**, *122*, 29228−29236.
(18) Uysal, A.; Rock, W.; Qiao, B. F.; Bu, W.; Lin, B. H. Two-Step Adsorption of PtCl62- Complexes at a Charged Langmuir Monolayer: Role of Hydration and Ion Correlations. *J. Phys. Chem. C* **2017**, *121*, 25377−25383.
(19) Scoppola, E.; Watkins, E. B.; Campbell, R. A.; Konovalov, O.; Girard, L.; Dufreche, J. F.; Ferru, G.; Fragneto, G.; Diat, O. Solvent Extraction: Structure of the Liquid-Liquid Interface Containing a Diamide Ligand. *Angew. Chem., Int. Ed.* **2016**, *55*, 9326−9330.
(20) Zhou, N. F.; Neuman, R. D. Dihexadecyl Phosphate Monolayers at the Heptane Water Interface - Model Interfacial System for Solvent-Extraction Studies. *Colloids Surf.* **1992**, *63*, 201−207.
(21) Kaganer, V. M.; Mohwald, H.; Dutta, P. Structure and phase transitions in Langmuir monolayers. *Rev. Mod. Phys.* **1999**, *71*, 779−819.
(22) Elderdfi, M.; Sikorski, A. F. Langmuir-monolayer methodologies for characterizing protein-lipid interactions. *Chem. Phys. Lipids* **2018**, *212*, 61−72.
(23) Ahlers, M.; Muller, W.; Reichert, A.; Ringsdorf, H.; Venzmer, J. Specific Interactions of Proteins with Functional Lipid Monolayers - Ways of Simulating Biomembrane Processes. *Angew. Chem., Int. Ed. Engl.* **1990**, *29*, 1269−1285.
(24) Dynarowicz-Łątka, P.; Dhanabalan, A.; Oliveira, O. N., Jr. Modern physicochemical research on Langmuir monolayers. *Adv. Colloid Interface Sci.* **2001**, *91*, 221−293.
(25) Giner-Casares, J. J.; Brezesinski, G.; Mohwald, H. Langmuir monolayers as unique physical models. *Curr. Opin. Colloid Interface Sci.* **2014**, *19*, 176−182.
(26) Stefaniu, C.; Brezesinski, G. X-ray investigation of monolayers formed at the soft air/water interface. *Curr. Opin. Colloid Interface Sci.* **2014**, *19*, 216−227.
(27) Sung, W.; Kim, D.; Shen, Y. R. Sum-frequency vibrational spectroscopic studies of Langmuir monolayers. *Curr. Appl. Phys.* **2013**, *13*, 619−632.
(28) Vollhardt, D. Brewster angle microscopy: A preferential method for mesoscopic characterization of monolayers at the air/water interface. *Curr. Opin. Colloid Interface Sci.* **2014**, *19*, 183−197.
(29) Li, D. Q. Development course of separating rare earths with acid phosphorus extractants: A critical review. *J. Rare Earths* **2019**, *37*, 468−486.
(30) Nash, K. L. The Chemistry of TALSPEAK: A Review of the Science. *Solvent Extr. Ion Exch.* **2015**, *33*, 1−55.
(31) Neuman, R. D.; Zhou, N. F.; Wu, J. G.; Jones, M. A.; Gaonkar, A. G.; Park, S. J.; Agrawal, M. L. General-Model for Aggregation of Metal-Extractant Complexes in Acidic Organophosphorus Solvent-Extraction Systems. *Sep. Sci. Technol.* **1990**, *25*, 1655−1674.
(32) Ibrahim, T. H. An Overview of the Physiochemical Nature of Metal-Extractant Species in Organic Solvent/Acidic Organophosphorus Extraction Systems. *Sep. Sci. Technol.* **2011**, *46*, 2157−2166.
(33) Steytler, D. C.; Jenta, T. R.; Robinson, B. H.; Eastoe, J.; Heenan, R. K. Structure of reversed micelles formed by metal salts of bis(ethylhexyl) phosphoric acid. *Langmuir* **1996**, *12*, 1483−1489.
(34) Grimes, T. S.; Jensen, M. P.; Debeer-Schmidt, L.; Littrell, K.; Nash, K. L. Small-angle neutron scattering study of organic-phase aggregation in the TALSPEAK process. *J. Phys. Chem. B* **2012**, *116*, 13722−13730.
(35) Kusaka, R.; Watanabe, M. Stoichiometry of Lanthanide-Phosphate Complexes at the Water Surface Studied Using Vibrational Sum Frequency Generation Spectroscopy and DFT Calculations. *J. Phys. Chem. B* **2021**, *125*, 6727−6731.
(36) Sun, P.; Binter, E. A.; Liang, Z.; Brown, M. A.; Gelis, A. V.; Benjamin, I.; Bera, M. K.; Lin, B.; Bu, W.; Schlossman, M. L. Antagonistic Role of Aqueous Complexation in the Solvent Extraction and Separation of Rare Earth Ions. *ACS Cent. Sci.* **2021**, *7*, 1908−1918.
(37) Bu, W.; Yu, H.; Luo, G.; Bera, M. K.; Hou, B.; Schuman, A. W.; Lin, B.; Meron, M.; Kuzmenko, I.; Antonio, M. R.; Soderholm, L.; Schlossman, M. L. Observation of a rare earth ion-extractant complex arrested at the oil-water interface during solvent extraction. *J. Phys. Chem. B* **2014**, *118*, 10662−10674.
(38) Bera, M. K.; Bu, W.; Uysal, A. Liquid Surface X-Ray Scattering. In *Physical Chemistry of Gas-Liquid Interfaces*, Elsevier, 2018; pp. 167−194.
(39) Pershan, P. S.; Schlossman, M., *Liquid Surfaces and Interfaces: Synchrotron X-ray Methods*. Cambridge University Press, 2012.
(40) Wang, W.; Park, R. Y.; Meyer, D. H.; Travesset, A.; Vaknin, D. Ionic specificity in pH regulated charged interfaces: Fe3+ versus La3+. *Langmuir* **2011**, *27*, 11917−11924.
(41) Kumal, R. R.; Nayak, S.; Bu, W.; Uysal, A. Chemical Potential Driven Reorganization of Anions between Stern and Diffuse Layers at the Air/Water Interface. *J. Phys. Chem. C* **2022**, *126*, 1140−1151.
(42) Sthoer, A.; Adams, E. M.; Sengupta, S.; Sanghamitra, S.; Corkery, R. W.; Allen, H. C.; Tyrode, E. C. La3+ and Y3+ interactions with the carboxylic acid moiety at the liquid/vapour interface:

https://doi.org/10.1021/acs.langmuir.2c00208
Langmuir 2022, 38, 5617−5625

identification of binding complexes, charge reversal, and detection limits. *J. Coll. Interface Sci.* **2022**, *608*, 2169−2180.
(43) Nayak, S.; Lovering, K.; Uysal, A. Ion-specific clustering of metal-amphiphile complexes in rare earth separations. *Nanoscale* **2020**, *12*, 20202−20210.
(44) Cotton, S. A.; Raithby, P. R. Systematics and surprises in lanthanide coordination chemistry. *Coord. Chem. Rev.* **2017**, *340*, 220−231.
(45) Seitz, M.; Oliver, A. G.; Raymond, K. N. The lanthanide contraction revisited. *J. Am. Chem. Soc.* **2007**, *129*, 11153−11160.
(46) Wilson, R. E.; Carter, T. J.; Autillo, M.; Stegman, S. Thiocyanate complexes of the lanthanides, Am and Cm. *Chem. Commun.* **2020**, *56*, 2622−2625.
(47) Dehnicke, K.; Greiner, A. Unusual complex chemistry of rare-earth elements: Large ionic radii-small coordination numbers. *Angew. Chem., Int. Ed.* **2003**, *42*, 1340−1354.
(48) Claesson, P.; Carmonaribeiro, A. M.; Kurihara, K. Dihexadecyl Phosphate Monolayers - Intralayer and Interlayer Interactions. *J. Phys. Chem. A* **1989**, *93*, 917−922.
(49) Bu, W.; Vaknin, D.; Travesset, A. How accurate is Poisson-Boltzmann theory for monovalent ions near highly charged interfaces? *Langmuir* **2006**, *22*, 5673−5681.
(50) Leontidis, E. Investigations of the Hofmeister series and other specific ion effects using lipid model systems. *Adv. Colloid Interface Sci.* **2017**, *243*, 8−22.
(51) Miller, M.; Chu, M.; Lin, B.; Meron, M.; Dutta, P. Observation of Ordered Structures in Counterion Layers near Wet Charged Surfaces: A Potential Mechanism for Charge Inversion. *Langmuir* **2016**, *32*, 73−77.
(52) Zhang, P.; Pham, T.; Zheng, X.; Liu, C.; Plata, P. L.; Kral, P.; Bu, W.; Lin, B.; Liu, Y. Spontaneous collapse of palmitic acid films on an alkaline buffer containing calcium ions. *Colloids Surf. B* **2020**, *193*, No. 111100.
(53) Travesset, A.; Vaknin, D. Bjerrum pairing correlations at charged interfaces. *Europhys. Lett.* **2006**, *74*, 181−187.
(54) Sung, W.; Vaknin, D.; Kim, D. Different Adsorption Behavior of Rare Earth and Metallic Ion Complexes on Langmuir Mono layers Probed by Sum-Frequency Generation Spectroscopy. *J. Opt. Soc. Korea* **2013**, *17*, 10−15.
(55) Servis, M. J.; Wu, D. T.; Shafer, J. C. The role of solvent and neutral organophosphorus extractant structure in their organization and association. *J. Mol. Liq.* **2018**, *253*, 314−325.
(56) Dul, M. C.; Braibant, B.; Dourdain, S.; Pellet-Rostaing, S.; Bourgeois, D.; Meyer, D. Perfluoroalkyl- vs alkyl substituted malonamides: Supramolecular effects and consequences for extraction of metals. *J. Fluorine Chem.* **2017**, *200*, 59−65.
(57) Vasudeva Rao, P. R.; Kolarik, Z. A review of third phase formation in extraction of actinides by neutral organophosphorus extractants. *Solvent Extr. Ion Exch.* **1996**, *14*, 955−993.
(58) Kolarik, Z. Review: Dissociation, Self-Association, and Partition of Monoacidic Organophosphorus Extractants. *Solvent Extr. Ion Exch.* **2010**, *28*, 707−763.
(59) Petrov, J. G.; Pfohl, T.; Mohwald, H. Ellipsometric chain length dependence of fatty acid Langmuir monolayers. A heads-and-tails model. *J. Phys. Chem. B* **1999**, *103*, 3417−3424.
(60) Li, M. Y.; Acero, A. A.; Huang, Z. Q.; Rice, S. A. Formation of an Ordered Langmuir Monolayer by a Nonpolar Chain Molecule. *Nature* **1994**, *367*, 151−153.
(61) Kusaka, R.; Watanabe, M. The structure of a lanthanide complex at an extractant/water interface studied using heterodyne-detected vibrational sum frequency generation. *Phys. Chem. Chem. Phys.* **2018**, *20*, 2809−2813.
(62) Phan, M. D.; Lee, J.; Shin, K. Collapsed States of Langmuir Monolayers. *J. Oleo. Sci.* **2016**, *65*, 385−397.
(63) Lee, K. Y. C. Collapse mechanisms of Langmuir monolayers. *Annu. Rev. Phys. Chem.* **2008**, *59*, 771−791.
(64) Bu, W.; Vaknin, D. Bilayer and trilayer crystalline formation by collapsing behenic acid monolayers at gas/aqueous interfaces. *Langmuir* **2008**, *24*, 441−447.
(65) Vaknin, D.; Bu, W.; Satija, S. K.; Travesset, A. Ordering by collapse: formation of bilayer and trilayer crystals by folding Langmuir monolayers. *Langmuir* **2007**, *23*, 1888−1897.
(66) Das, K.; Sah, B. K.; Kundu, S. Cation-induced monolayer collapse at lower surface pressure follows specific headgroup percolation. *Phys. Rev. E* **2017**, *95*, No. 022804.
(67) Heimburg, T. Lipid ion channels. *Biophys. Chem.* **2010**, *150*, 2−22.
(68) Redondo-Morata, L.; Giannotti, M. I.; Sanz, F. Structural impact of cations on lipid bilayer models: nanomechanical properties by AFM-force spectroscopy. *Mol. Membr. Biol.* **2014**, *31*, 17−28.
(69) Matsuzaki, K.; Yoneyama, S.; Murase, O.; Miyajima, K. Transbilayer transport of ions and lipids coupled with mastoparan X translocation. *Biochemistry* **1996**, *35*, 8450−8456.
(70) Lin, J.; Dargazany, R.; Alexander-Katz, A. Lipid Flip-Flop and Pore Nucleation on Zwitterionic Bilayers are Asymmetric under Ionic Imbalance. *Small* **2017**, *13*, No. 1603708.
(71) Ma, Y. H.; Li, B. L.; Yang, J. J.; Han, X. F.; Chen, Z.; Lu, X. L. Metal Ion Size-Dependent Effects on Lipid Transmembrane Flip-Flop. *J. Phys. Chem. C* **2019**, *123*, 17899−17907.
(72) Matile, S.; Nakanishi, K. Selective cation movement across lipid bilayers containing brevetoxin B. *Angew. Chem. Int. Ed. Engl.* **1996**, *35*, 757−759.
(73) Moradi, M.; Lengweiler, N. L.; Housecroft, C. E.; Tulli, L. G.; Stahlberg, H.; Jung, T. A.; Shahgaldian, P. Coordination-Driven Monolayer-to-Bilayer Transition in Two-Dimensional Metal-Organic Networks. *J. Phys. Chem. B* **2021**, *125*, 4204−4211.
(74) Yoo, S.; Qiao, B.; Douglas, T.; Bu, W.; Olvera de la Cruz, M.; Dutta, P. Specific Ion Effects in Lanthanide−Amphiphile Structures at the Air−Water Interface and Their Implications for Selective Separation. *ACS Appl. Mater. Interfaces* **2022**, *14*, 7504−7512.
(75) Vollhardt, D.; Retter, U. Nucleation in Insoluble Monolayers. 1. Nucleation and Growth-Model for Relaxation of Metastable Monolayers. *J. Phys. Chem. B* **1991**, *95*, 3723−3727.
(76) Danauskas, S. M.; Li, D. X.; Meron, M.; Lin, B. H.; Lee, K. Y. C. Stochastic fitting of specular X-ray reflectivity data using StochFit. *J. Appl. Crystallogr.* **2008**, *41*, 1187−1193.

https://doi.org/10.1021/acs.langmuir.2c00208
Langmuir 2022, 38, 5617−5625